ACS OMEGA

http://pubs.acs.org/journal/acsodf

Article

Role of a Solution-Processed V_2O_5 Hole Extracting Layer on the Performance of CuO-ZnO-Based Solar Cells

Shamim Ahmmed,* Asma Aktar, and Abu Bakar Md. Ismail*

Cite This: *ACS Omega* 2021, 6, 12631−12639

Read Online

ACCESS | Metrics & More | Article Recommendations | Supporting Information

ABSTRACT: In this research, a heterostructure of the CuO-ZnO-based solar cells has been fabricated using low-cost, earth-abundant, non-toxic metal oxides by a low-cost, low-temperature spin coating technique. The device based on CuO-ZnO without a hole transport layer (HTL) suffers from poor power conversion efficiency due to carrier recombination on the surface of CuO and bad ohmic contact between the metal electrode and the CuO absorber layer. The main focus of this research is to minimize the mentioned shortcomings by a novel idea of introducing a solution-processed vanadium pentoxide (V_2O_5) HTL in the heterostructure of the CuO-ZnO-based solar cells. A simple and low-cost spin coating technique has been investigated to deposit V_2O_5 onto the absorber layer of the solar cell. The influence of the V_2O_5 HTL on the performance of CuO-ZnO-based solar cells has been investigated. The photovoltaic parameters of the CuO-ZnO-based solar cells were dramatically enhanced after insertion of the V_2O_5 HTL. V_2O_5 was found to enhance the open-circuit voltage of the CuO-ZnO-based solar cells up to 231 mV. A detailed study on the effect of defect properties of the CuO absorber layer on the device performance was theoretically accomplished to provide future guidelines for the performance enhancement of the CuO-ZnO-based solar cells. The experimental results indicate that solution-processed V_2O_5 could be a promising HTL for the low-cost, environment-friendly CuO-ZnO-based solar cells.

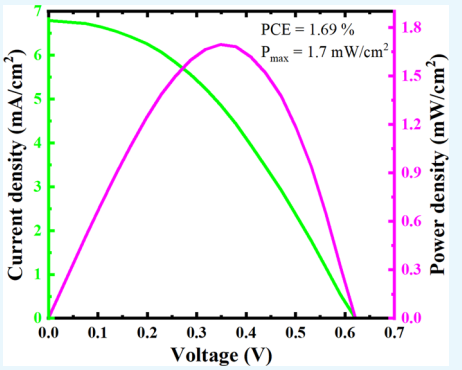

1. INTRODUCTION

Solar energy is one of the largest, flexible, and technologically advanced, sustainable, low-carbon choices available to satisfy the increasing global electric power demand. Photovoltaic devices are the most extensively used solar technology to utilize solar power. Electricity from photovoltaics could fill around 20% of the market for global primary energy by 2050.[1] Crystalline silicon (c-Si) is the most successful photovoltaic technology available, which occupies about 90% of the current world photovoltaic market share.[2] The cost per efficiency of the silicon solar cells is the main concerning issue to the photovoltaic researcher community.[3] This issue has driven the researchers toward finding an alternative earth-abundant absorber material for the fabrication of low-cost highly efficient solar cells.

Inorganic metal oxides (IMOs) are earth-abundant materials and can be synthesized using very simple and low-cost environment-friendly chemical routes. With band gaps of 1.34−1.7 eV and a high absorption coefficient, CuO, a p-type IMO, could be one of the promising candidates for photovoltaic applications.[4,5] CuO has some other excellent features like high minority carrier diffusion length,[6] tunable electrical properties,[7] etc. These features of CuO have enabled its use in the sensor,[8−12] photoelectrochemical cell,[13−16] capacitive device,[17−21] and photovoltaic[5,22−26] applications. According to the Shockley−Queisser limit, ∼30% power conversion efficiency (PCE) could be obtained from the single-junction CuO-based solar cells.[20]

A suitable n-type material is required with the CuO absorber layer for the formation of a single p−n junction CuO-based solar cell. ZnO is an extensively used electron transport material in low-cost highly efficient solar cells.[27−29] It is an earth-abundant, non-toxic, and wide band gap n-type IMO with high electron mobility.[30] The energy band alignment of n-type ZnO is suitably matched with p-type CuO.[31,32] Therefore, ZnO could be a promising electron transport layer (ETL) for the CuO-based solar cells. Furthermore, few research groups have experimented on ZnO-CuO-based solar cells in recent years, but the reported efficiency of these solar cells is very low.[5,33−36] There are many effective ways to improve the performance of the heterojunction solar cell (HSC) like band gap tuning,[37,38] band alignment engineering,[5,39] crystallinity improvement of the absorber layer,[40] use of charge-selective layers,[41−43] etc. Kaphle and co-workers have worked on the band alignment engineering of the ZnO-CuO-based hetero-

Received: February 5, 2021
Accepted: April 26, 2021
Published: May 4, 2021

junction solar cell and observed a considerable performance improvement.[5] Kuddus et al. have researched on the performance enhancement of the ZnO-CuO-based heterojunction solar cell through the band gap tuning of CuO using a silicon nanoparticle (Si-NP) dopant.[36] Naveena et al. have also experimented on the band gap tuning of CuO using an ytterbium (Yb) dopant and observed a significant role of this technique on the performance enhancement of the ZnO-CuO-based heterojunction solar cell.[34]

The introduction of a hole transport layer (HTL) has been found to be an effective technique for the performance enhancement of the heterojunction solar cell.[44,45] Recently, attractive featured transition metal oxides (TMOs) such as nickel oxide (NiO),[46,47] tungsten trioxide (WO_3),[48,49] cuprous oxide (Cu_2O),[50,51] molybdenum trioxide (MoO_3),[52,53] and vanadium pentoxide (V_2O_5)[54−56] have been used in the different organic and inorganic solar cells as the HTL. The low resistive contact with the active layer, high optical transparency in the visible range, good stability at ambient conditions, a wide range of band alignments, and feasible deposition by a facile solution process are the most fascinating features of these TMOs.[57−59] Kaphle et al. have found a significant performance enhancement after the introduction of the MoO_3 HTL in a practical structure of the ZnO-CuO-based solar cell.[5] Recently, Lam has conducted a numerical study on the planar ZnO-CuO based-solar cell using the Cu_2O HTL and reported a maximum achievable PCE of 12.18%.[26] The valence band maximum (VBM) and the conduction band maximum (CBM) of V_2O_5 are suitably matched with the VBM and the CBM of CuO, which could accelerate the hole transport from the CuO absorber layer to the output terminal of the solar cell as well as block the photogenerated electrons at the CuO/V_2O_5 interface.[55,60] Therefore, V_2O_5 could be a potential hole extracting layer for the ZnO/CuO-based solar cell.

Simulation is a widely accepted technique for device modeling, performance analysis, and understanding the overall device physics of the designed heterojunction solar cells.[61] The key advantage of the numerical simulation is that the effect of different physical parameters of the materials on the device performance can be easily investigated. Such a type of investigation provides the guidelines to obtain optimum performance from a designed solar cell without fabricating it in the laboratory. For numerical simulation of heterojunction solar cells, a solar cell capacitance simulator (SCAPS),[61,62] analysis of microelectronic and photonic structures (AMPS),[63,64] and Silvaco TCAD[65,66] have been popularly used in recent years.

In this research, low-cost CuO-ZnO-based solar cells have been successfully fabricated using the spin coating technique. The solution-processed V_2O_5 HTL has been introduced in the CuO-ZnO-based solar cells. V_2O_5 has dramatically boosted the V_{OC} and device performance. A numerical simulation on the defect features of the CuO absorber layer has also been conducted using the SCAPS simulation program. A maximum PCE of 1.69% has been recorded from the experimented CuO-ZnO-based solar cell.

2. RESULTS AND DISCUSSION

2.1. Structural Properties. ZnO, CuO, and V_2O_5 thin films were fabricated using prepared ZnO, CuO, and V_2O_5 solutions (Section 4.2), respectively, and annealed at a temperature of 300 °C for 1 h in open air. XRD analysis of these films was done for the confirmation of ZnO, CuO, and V_2O_5, shown in Figure 1. From Figure 1, it is seen that the peaks at 2θ values of 31.84, 34.52, 36.38, 47.64, and 56.7° correspond to (100), (002), (101), (102), and (110) planes evident to the ZnO wurtzite crystal structure (JCPDS card no. 36-1451). CuO confirmation peaks at 32.5, 35.4, 35.5, 38.7, and 48.7° correspond to (110), (002), ($\bar{1}$11), (111), and ($\bar{2}$02) planes, and these planes have revealed the monoclinic crystal structure of CuO (JCPDS card no. 48-1548). In Figure 1, the sharp peak at a 2θ value of 20.12° corresponds to the (010) plane, which indicates the orthorhombic structure of V_2O_5 (JCPDS card no. 01-076-1803). The fabricated V_2O_5 film was also polycrystalline in nature. There are some peaks of V_2O_5 that are not clear in Figure 1 due to their low intensity.

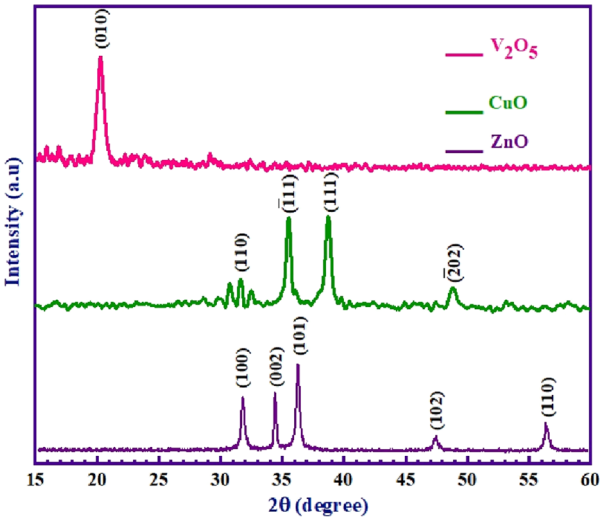

Figure 1. XRD patterns of the fabricated ZnO, CuO, and V_2O_5 thin films annealed at 300 °C.

The cell performance is strongly dependent on the surface morphology of the HTL that defines the interface between the absorber layer (CuO) and the back metal contact (Ag).[67] SEM was performed to analyze the top surface morphology of two-layer V_2O_5 on top of the CuO-ZnO-based HSC, shown in Figure 2. A compressed, quite uniform, and almost pinhole-free surface of V_2O_5 on CuO is observed from Figure 2. A similar surface is expected to form at the back side of V_2O_5 at the

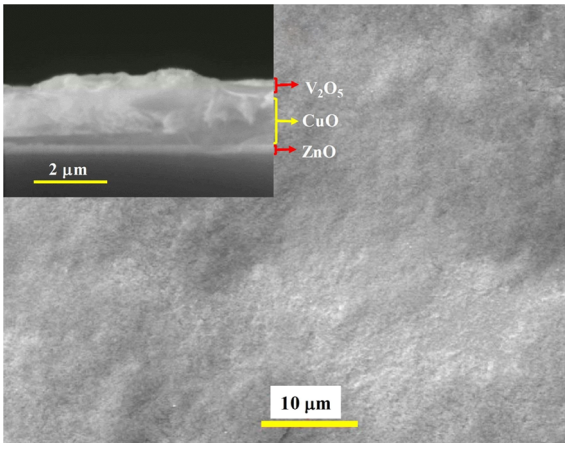

Figure 2. Top surface and cross-sectional SEM image of the CuO-ZnO-based HSC with the two-layer V_2O_5 HTL.

https://doi.org/10.1021/acsomega.1c00678
ACS Omega 2021, 6, 12631−12639

CuO/V_2O_5 interface. Therefore, the CuO/V_2O_5 interface as well as the V_2O_5/Ag interface could help to form a good ohmic contact between the CuO absorber layer and the Ag back contact, which in turn will reduce the device series resistance.

The chemical compositions present in the CuO-ZnO-based HSC with the two-layer V_2O_5 HTL were analyzed using EDS, which are listed in Table 1. Table 1 indicates that oxygen (O), vanadium (V), copper (Cu), zinc (Zn), indium (In), and tin (Sn) were present in the CuO-ZnO-based HSC with the two-layer V_2O_5 HTL.

Table 1. Elemental Composition of the CuO-ZnO-Based HSC with the Two-Layer V_2O_5 HTL Observed from the EDS Spectra

element	Zn	Cu	V	O	In	Sn
weight %	12.07	45.73	10.51	16.28	1.29	14.13
atomic %	8.17	31.85	9.13	45.08	0.5	5.27

2.2. Optical Properties. The optical transmittance spectra of V_2O_5 thin films annealed at 250, 300, and 350 °C in open air for 1 h are illustrated in Figure 3. It is observed that the transmittance increases between the wavelength of 520 and1100 nm with increasing the annealing temperature, which is due to the thermochromism property of V_2O_5.[68] The optical band gap has been found to be around 2.45, 2.4, and 2.3 eV from the V_2O_5 thin films annealed at 250, 300, and 350 °C, respectively, by using the Tauc formula, $(\alpha h\upsilon)^2 = c(h\upsilon - E_g)$, which is depicted in Figure 3b. The variation of the band gap might be due to the change of stoichiometry of V_2O_5 with the temperature change.

2.3. Electrical Properties. The energy band diagram and the schematic diagram of the CuO-ZnO-based HSCs with the V_2O_5 HTL are depicted in Figure 4. The junction property of the CuO-ZnO-based HSC with two-layer V_2O_5 was characterized by capacitance−voltage ($C-V$) measurement using an impedance analyzer. Figure 5 delineates the Mott−Schottky plot of the CuO-ZnO-based HSC with the two-layer V_2O_5 HTL. The ascertainment of the built-in potential (ψ_{bi}) of the CuO-ZnO-based HSC with V_2O_5 was done by fitting and extrapolating the linear portion of the plots, and ψ_{bi} was found

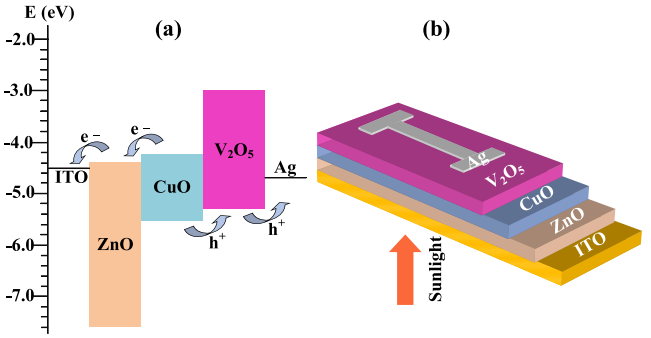

Figure 4. (a) Energy band diagram and (b) schematic diagram of the CuO-ZnO-based HSCs with the V_2O_5 HTL.

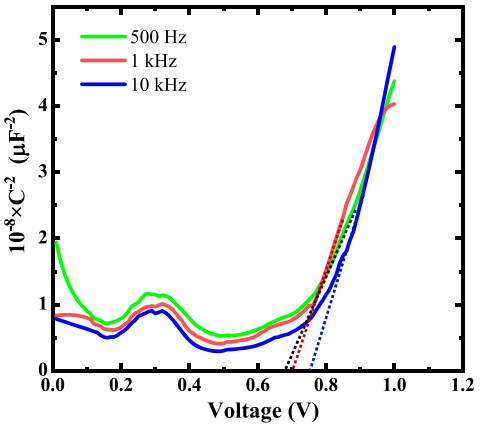

Figure 5. Mott−Schottky plot of the CuO-ZnO-based HSC with the two-layer HTL at frequencies of 500 Hz, 1 kHz, and 10 kHz.

to vary from 0.68 to 0.76 V at frequencies of 500 Hz, 1 kHz, and 10 kHz. According to the p−n junction solar cell theory, the built-in potential is nearly equal to the open-circuit voltage (V_{oc}) under a sunlight illumination of 100 mW/cm^2.[69]

The $J-V$ characteristics of the fabricated CuO-ZnO-based HSCs with and without V_2O_5 were investigated under an illumination of 1.5 AM (100 mW/cm^2) simulated sunlight conditions. As the main focus of this research is to observe the

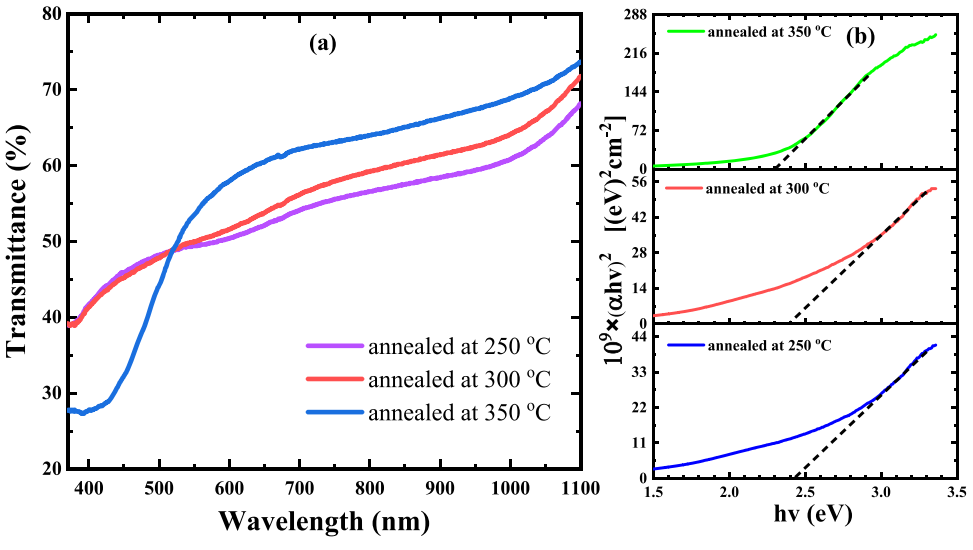

Figure 3. (a) Optical transmittance spectra and (b) Tauc plots of V_2O_5 thin films annealed at 250, 300, and 350 °C.

https://doi.org/10.1021/acsomega.1c00678
ACS Omega 2021, 6, 12631−12639

influence of the solution-processed V_2O_5 HTL on the performance of CuO-ZnO-based HSCs, different parameters of V_2O_5 like thickness and deposition temperature should be optimized. Here, the thickness of V_2O_5 was experimented with the number of deposited layers keeping deposition temperature constant. Figure 6 depicts the $J-V$ characteristics of

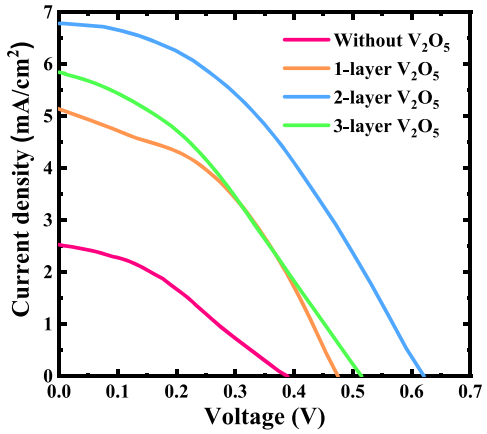

Figure 6. $J-V$ curve of CuO-ZnO-based HSCs without the V_2O_5 HTL and with one-layer, two-layer, and three-layer V_2O_5 HTLs.

CuO-ZnO-based HSCs without the V_2O_5 HTL and with one-layer, two-layer, and three-layer V_2O_5 HTLs. All the photovoltaic parameters were significantly improved after the insertion of the V_2O_5 HTL in between the CuO absorber layer and the Ag electrode of the CuO-ZnO-based HSCs. The solar cell with a two-layer V_2O_5 HTL showed optimum performance. The CuO-ZnO HSC without a V_2O_5 HTL exhibited a V_{OC}, J_{SC}, fill factor (FF), and PCE of 0.389 V, 2.54 mA/cm^2, 34%, and 0.332%, respectively. Meanwhile, a maximum PCE of 1.69% with a V_{OC}, J_{SC}, and FF of 0.62 V, 6.78 mA/cm^2, and 40.2%, respectively, was observed from the CuO-ZnO-based HSC with a two-layer V_2O_5 HTL. The thickness of the two-layer V_2O_5 HTL was around 230 nm, which was measured from the cross-sectional SEM image shown in Figure 2. It is observed from Figure 6 that the V_{OC} of the CuO-ZnO-based HSC with two-layer V_2O_5 is very close to its built-in potential estimated from the Mott–Schottky plot (shown in Figure 5). This close match of built-in potential with the V_{OC} indicates that the losses of built-in potential were compensated after insertion of the V_2O_5 HTL due to the formation of a good ohmic contact with the Ag electrode.

The photovoltaic parameters with the number of the deposited V_2O_5 layer are listed in Table 2. It is observed from Table 2 that the V_{OC}, J_{SC}, FF, and PCE change with the deposited layer number of the V_2O_5 HTL, which might be due to the change of series and shunt resistance of the solar cell.[70]

Table 2. The Comparison of Photovoltaic Parameters of CuO-ZnO-Based Inorganic Thin-Film HSCs with Different Thicknesses of the V_2O_5 Hole Transport Layer

V_2O_5 layer number	V_{OC} (V)	J_{SC} (mA/cm^2)	FF (%)	PCE (%)	R_S (Ω cm^2)
0	0.389	2.54	34	0.332	122
1	0.475	5.18	42	1.029	44
2	0.62	6.78	40.2	1.69	28
3	0.515	5.87	35	1.054	57

Generally, the series resistance (R_S) of the solar cell comes from the absorber layer and contact electrodes.[71] The insertion of the V_2O_5 HTL creates two interfaces CuO/V_2O_5 and V_2O_5/Ag, and these interfaces might contribute to the lowering of the series resistance of the ITO/ZnO/CuO/V_2O_5/Ag heterostructure. The series resistance (R_S) of the CuO-ZnO-based HSCs without and with the V_2O_5 HTL was estimated from the slope of the $J-V$ curve at a current density (J) of 0 mA/cm^2 and is listed in Table 2. The estimated series resistance indicates that the two-layer V_2O_5 HTL remarkably reduced the contact resistance around three times.

2.4. Theoretical Analysis of Defect Properties of the CuO Absorber Layer. The non-radiative Shockley–Read–Hall (SRH) recombination is the main factor that is responsible for most of the power loss in photovoltaics.[72] The presence of the deep level defect in the absorber layer is the primary source of the SRH recombination.[73] High defect density in the absorber layer reduces the photogenerated carrier lifetime and device performance. SRH recombination can be defined by the following equation

$$R_{SRH} = \frac{np - n_i^2}{\tau\left(p + n - 2n_i\cosh\left(\frac{E_i - E_A}{kT}\right)\right)} \quad (1)$$

where τ, E_A, k, and T are the carrier lifetime, defect activation energy level, Boltzmann constant, and device working temperature, respectively.

Carrier lifetime can be estimated using the following equation

$$\tau = \frac{1}{\sigma \times N_t \times V_{th}} \quad (2)$$

where σ, N_t, and V_{th} are the carrier capture cross section, defect density, and thermal velocity of the carrier, respectively.

The fabricated CuO-ZnO-based HSC with two-layer V_2O_5 was theoretically validated using the SCAPS simulation tool. The $J-V$ characteristics and quantum efficiency curves of the theoretically validated device are depicted in Figure S2. The whole simulation study was conducted using the default parameters listed in Table S1. The CuO absorber layer defect properties were numerically analyzed using the SCAPS simulation program. The photovoltaic performance of the theoretically validated CuO-ZnO-based HSC was studied by varying the CuO absorber layer thickness from 400 to 1400 nm and CuO deep level defect density from 10^{10} to 10^{18} cm^{-3}, while the hole capture cross section (σ_p) and defect activation energy (E_A) were kept constant at 10^{-15} cm^2 and 0.6 eV, respectively. It is observed from Figure 7c that the V_{OC} decreases with the increase in defect density above 10^{14} cm^{-3}. Figure 7a indicates that the SRH recombination increases with the increase in defect density, which in turn increases the non-radiative loss of the V_{OC}.[74] It is also obvious from Figure 7b that the carrier lifetime at the CuO absorber layer decreases with the defect density. Figure 7 indicates that the defect density up to 10^{14} cm^{-3} is tolerable and above which PCE is drastically reduced with the defect density.

From eqs 1 and 2, it is clear that the E_A and hole capture cross section σ_p of the CuO absorber layer have a considerable effect on the SRH recombination and the carrier lifetime. It is observed from Figure 8a that the SRH recombination increases with the E_A. As shown in Figure 8b, the carrier lifetime decreases with σ_p. The performance of the theoretically

https://doi.org/10.1021/acsomega.1c00678
ACS Omega 2021, 6, 12631–12639

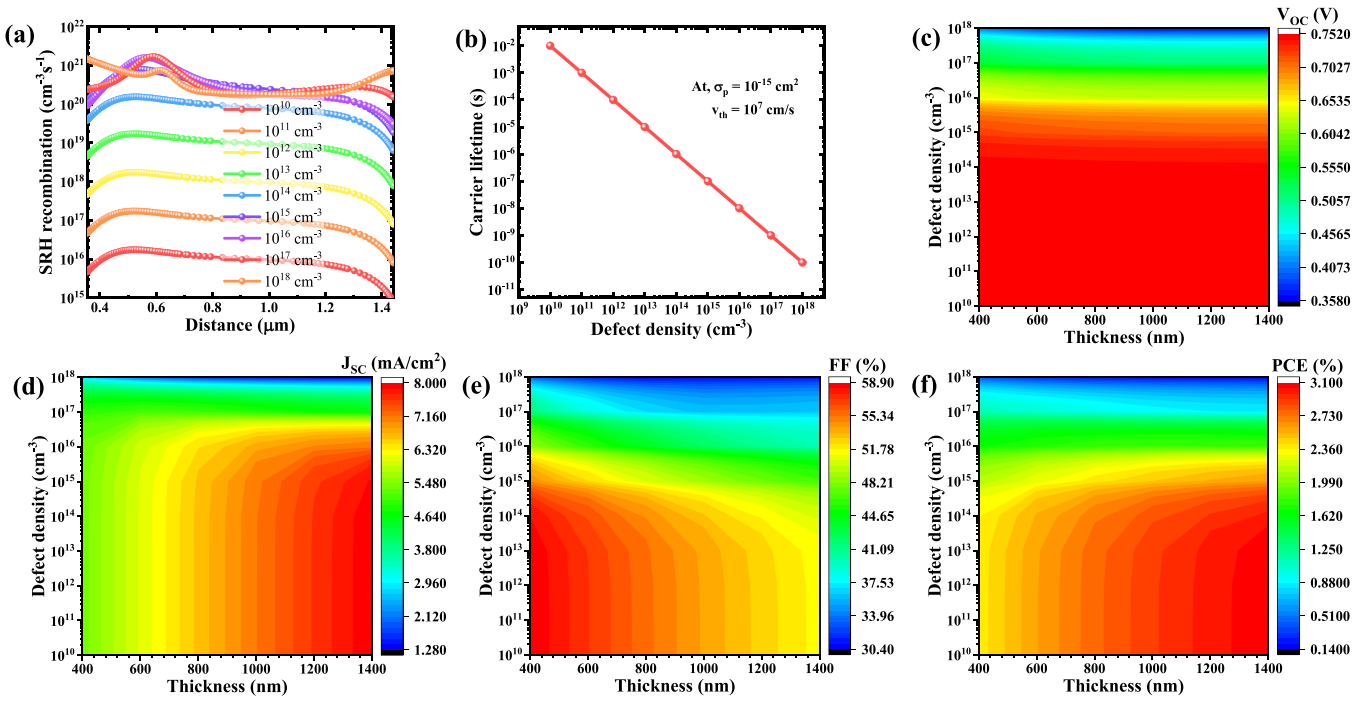

Figure 7. Variation of (a) SRH recombination and (b) carrier lifetime at the CuO layer with deep level defect density of the CuO absorber layer and (c–f) photovoltaic parameters of the CuO-ZnO-based HSC as a function of thickness and deep level defect density of the CuO absorber layer.

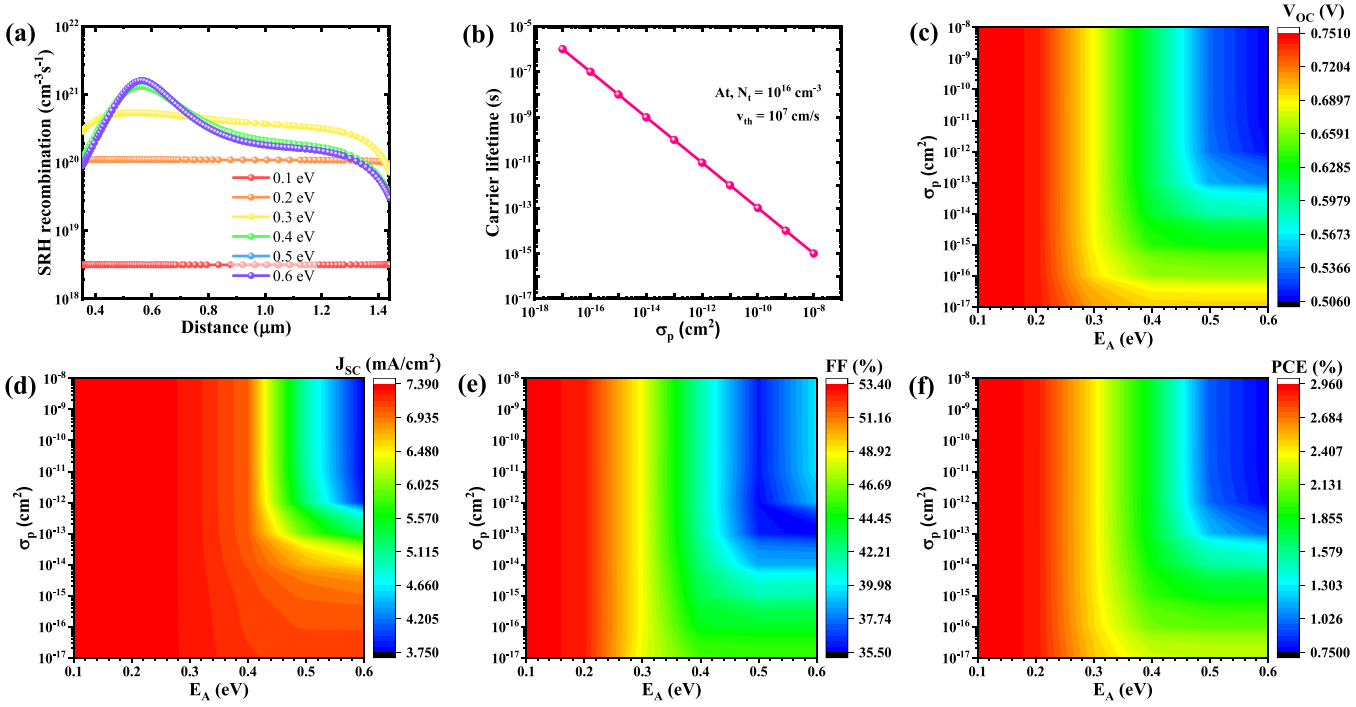

Figure 8. Variation of (a) SRH recombination at the CuO layer with E_A, (b) carrier lifetime at the CuO layer with σ_p, and (c–f) photovoltaic parameters of the CuO-ZnO-based HSC as a function of E_A and σ_p of the CuO absorber layer.

validated CuO-ZnO-based HSC was investigated by varying E_A from 0.1 to 0.6 eV (above E_V) and σ_p from 10^{-17} to 10^{-8} cm^2, while the defect density of the CuO layer was kept constant at 10^{16} cm^{-3}. As shown in Figure 8c,f, the V_{OC} and PCE are almost independent of the σ_p till an E_A of 0.2 eV, while the V_{OC} and PCE decrease with increasing E_A above 0.2 eV. The E_A-assisted decrement of the V_{OC} and PCE is consistent with the variation of SRH recombination, which is shown in Figure 8a. The effect of σ_p was found to be dominant at E_A > 0.45 eV. Figure S3 indicates that the optical loss at the front surface of the CuO-ZnO-based HSC is another factor that is responsible for the low performance besides the defect properties of the CuO absorber layer.

https://doi.org/10.1021/acsomega.1c00678
ACS Omega 2021, 6, 12631−12639

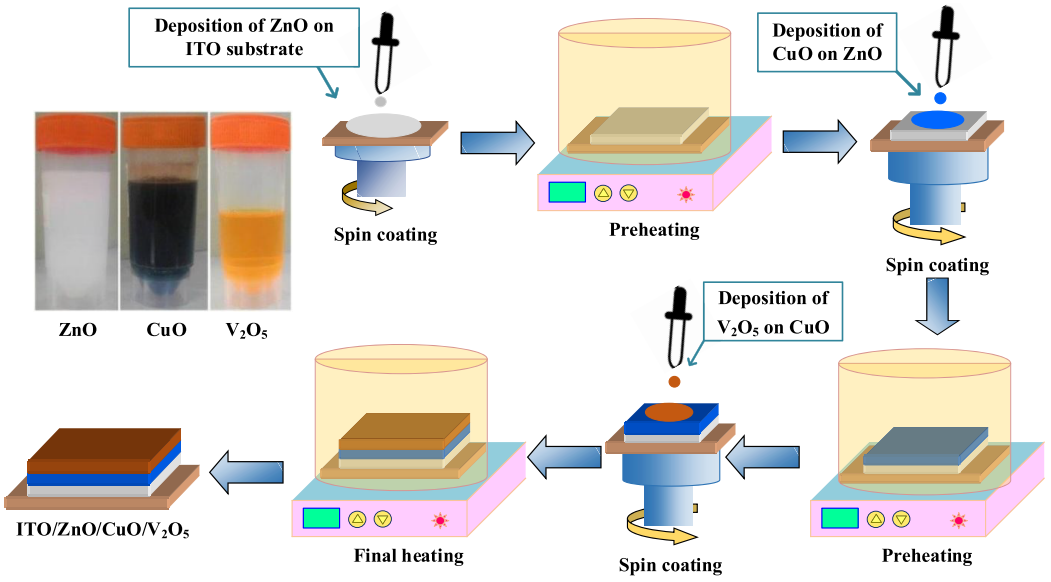

Figure 9. Flow diagram of the CuO-ZnO-based heterojunction solar cell fabrication process.

3. CONCLUSIONS

Low-cost environment-friendly CuO-ZnO-based solar cells have been successfully fabricated using a facile chemical route. The solution-processed V_2O_5 HTL has been inserted in the heterostructure of the CuO-ZnO solar cells using the spin coating technique. The V_{OC} was enhanced up to 231 mV after deposition of the V_2O_5 HTL in between the CuO and Ag electrode, which indicates that the V_2O_5 HTL has significantly reduced the non-radiative SRH recombination at the CuO surface. The performance of the CuO-ZnO-based solar cells has also been numerically investigated using the SCAPS simulation tool. It is obvious from the numerical investigations that the CuO absorber layer defect parameters like N_t, E_A, and σ_p have a huge impact on the device performance. The overall findings indicate that solution-processed V_2O_5 could be a potential HTL for the low-cost CuO-ZnO-based solar cells.

4. EXPERIMENTAL SECTION

4.1. Materials. Diethanolamine (DEA, ≥98.0%), ethanol (CH_3CH_2OH, 96%), zinc acetate dihydrate [$Zn(CH_3COO)_2 \cdot 2H_2O$, 99.999%], copper acetate monohydrate [$Cu(CH_3COO)_2 \cdot H_2O$, ≥99%], vanadium pentoxide (V_2O_5, 99.95%), and indium tin oxide (ITO)-coated glass substrates (surface resistivity of around 8−12 Ω/sq) were purchased from Sigma-Aldrich. All chemicals were used without further purification.

4.2. Solution Preparation. The ZnO solution was prepared by dissolving 0.65 g of zinc acetate dihydrate in 20 mL of ethanol. Then, the solution was stirred with the help of a magnetic stirrer at 40 °C for the next 10 min. After that, 1 mL of diethanolamine (DEA) as a stabilizer was added to this solution, and the solution was also stirred for the next 30 min at a temperature of 40 °C. Hence, a homogeneous solution of ZnO was obtained. Applying a similar process, 0.6 g of copper acetate monohydrate, 2 mL of DEA, and 20 mL of ethanol were used to prepare the CuO solution. By a similar process, the V_2O_5 solution was also prepared with 0.25 g of vanadium oxide powder, 2 mL of DEA, and 20 mL of ethanol.

4.3. Cell Fabrication. The ITO glass substrates were used to fabricate the HSCs. Before fabrication, the ITO glass substrates were cleaned in an ultrasonic vibrator using acetone, isopropanol, and distilled water for 15 min in sequence. Then, the cleaned ITO glass substrate was placed on a spin coating system, and 10 μL of the ZnO solution was drop cast on the ITO glass substrate and spun for 30s at 1500 rpm. The film was preheated at 150 °C for 10 min, and this process was repeated for the deposition of each layer of ZnO. A similar process was adopted for the deposition of the absorber layer of CuO on the ZnO layer. Finally, after annealing at 300 °C for 1 h in open air, the ZnO-CuO-based HSC without an HTL was fabricated. A patterned Ag paste was used to make the back-side contact of the solar cells. Through a similar process, the ZnO-CuO-based heterojunction solar cell with an HTL was fabricated. The prepared solution of V_2O_5 was deposited on the CuO layer as an HTL by spin coating, and finally, the film was annealed at 300 °C for 1 h in open air. The fabrication flow diagram is shown in Figure 9.

4.4. Characterization. The crystallographic analysis of XRD patterns of ZnO, CuO, and V_2O_5 thin films was done using an X-ray diffractometer (GBC, εMMA) with monochromatic Cu Kα radiation having a wavelength of 1.540598 Å. SEM images were also taken using a scanning electron microscope (SEM, Zeiss, EVO 18). Energy-dispersive X-ray spectroscopy (EDAX, AMETEK) in SEM was performed to analyze chemical compositions present in ITO/ZnO/CuO/V_2O_5. Transmittance spectra of V_2O_5 thin films were measured by T-60 UV−visible spectroscopy, and current density versus voltage ($J-V$) of the fabricated solar cells was measured using a Keithley 2400 source meter under an illumination of 1.5 AM simulated light. All characterizations were conducted at room temperature (~27 °C) and a relative humidity (RH) of ~50%.

■ ASSOCIATED CONTENT

Supporting Information

The Supporting Information is available free of charge at https://pubs.acs.org/doi/10.1021/acsomega.1c00678.

Physical parameters used in the simulation (Table S1); absorption coefficients of ZnO, CuO, and V_2O_5 (Figure S1); $J-V$ characteristics and QE curve of the theoretically validated CuO-ZnO-based HSC (Figure

https://doi.org/10.1021/acsomega.1c00678
ACS Omega 2021, 6, 12631−12639

S2); and $J-V$ characteristics of the theoretically validated CuO-ZnO-based HSC for various optical losses (Figure S3) (PDF)

AUTHOR INFORMATION

Corresponding Authors

Shamim Ahmmed − *Solar Energy Laboratory, Department of Electrical and Electronic Engineering, University of Rajshahi, Rajshahi 6205, Bangladesh; Department of Electrical and Electronic Engineering, North Bengal International University, Rajshahi 6100, Bangladesh;* orcid.org/0000-0001-5847-2893; Email: shamim.apee.ru@gmail.com

Abu Bakar Md. Ismail − *Solar Energy Laboratory, Department of Electrical and Electronic Engineering, University of Rajshahi, Rajshahi 6205, Bangladesh;* orcid.org/0000-0001-6856-5663; Email: ismail@ru.ac.bd

Author

Asma Aktar − *Solar Energy Laboratory, Department of Electrical and Electronic Engineering, University of Rajshahi, Rajshahi 6205, Bangladesh;* orcid.org/0000-0002-7391-9849

Complete contact information is available at: https://pubs.acs.org/10.1021/acsomega.1c00678

Notes

The authors declare no competing financial interest.

ACKNOWLEDGMENTS

The authors gratefully acknowledge financial support from the ICT Division, Ministry of Posts, Telecommunications and IT, Government of the People's Republic of Bangladesh.

REFERENCES

(1) International Renewable Energy Agency (IRENA). *Global Energy Transformation (GET): A Roadmap to 2050*; 2019.

(2) Battaglia, C.; Cuevas, A.; De Wolf, S. High-Efficiency Crystalline Silicon Solar Cells: Status and Perspectives. *Energy Environ. Sci.* **2016**, *9*, 1552−1576.

(3) Kumar Dalapati, G.; Masudy-Panah, S.; Kumar, A.; Cheh Tan, C.; Ru Tan, H.; Chi, D. Aluminium Alloyed Iron-Silicide/Silicon Solar Cells: A Simple Approach for Low Cost Environmental-Friendly Photovoltaic Technology. *Sci. Rep.* **2016**, *5*, 17810.

(4) Kampmann, J.; Betzler, S.; Hajiyani, H.; Häringer, S.; Beetz, M.; Harzer, T.; Kraus, J.; Lotsch, B. V.; Scheu, C.; Pentcheva, R.; Fattakhova-Rohlfing, D.; Bein, T. How Photocorrosion Can Trick You: A Detailed Study on Low-Bandgap Li Doped CuO Photocathodes for Solar Hydrogen Production. *Nanoscale* **2020**, *12*, 7766−7775.

(5) Kaphle, A.; Echeverria, E.; Mcllroy, D. N.; Hari, P. Enhancement in the Performance of Nanostructured CuO−ZnO Solar Cells by Band Alignment. *RSC Adv.* **2020**, *10*, 7839−7854.

(6) Sawicka-Chudy, P.; Sibiński, M.; Rybak-Wilusz, E.; Cholewa, M.; Wisz, G.; Yavorskyi, R. Review of the Development of Copper Oxides with Titanium Dioxide Thin-Film Solar Cells. *AIP Adv.* **2020**, *10*, No. 010701.

(7) Lu, Y.; Yan, H.; Qiu, K.; Cheng, J.; Wang, W.; Liu, X.; Tang, C.; Kim, J.-K.; Luo, Y. Hierarchical Porous CuO Nanostructures with Tunable Properties for High Performance Supercapacitors. *RSC Adv.* **2015**, *5*, 10773−10781.

(8) Yang, F.; Guo, J.; Liu, M.; Yu, S.; Yan, N.; Li, J.; Guo, Z. Design and Understanding of a High-Performance Gas Sensing Material Based on Copper Oxide Nanowires Exfoliated from a Copper Mesh Substrate. *J. Mater. Chem. A* **2015**, *3*, 20477−20481.

(9) Wang, S.; Gao, Z.; Song, G.; Yu, Y.; He, W.; Li, L.; Wang, T.; Fan, F.; Li, Y.; Zhang, L.; Zhang, X.; Fu, Y.; Qi, W. Copper Oxide Hierarchical Morphology Derived from MOF Precursors for Enhancing Ethanol Vapor Sensing Performance. *J. Mater. Chem. C* **2020**, *8*, 9671−9677.

(10) Zhang, P.-P.; Zhang, H.; Sun, X.-H. A Uniform Porous Multilayer-Junction Thin Film for Enhanced Gas-Sensing Performance. *Nanoscale* **2016**, *8*, 1430−1436.

(11) Lee, J. E.; Lim, C. K.; Park, H. J.; Song, H.; Choi, S.-Y.; Lee, D.-S. ZnO−CuO Core-Hollow Cube Nanostructures for Highly Sensitive Acetone Gas Sensors at the Ppb Level. *ACS Appl. Mater. Interfaces* **2020**, *12*, 35688−35697.

(12) Mali, S. M.; Narwade, S. S.; Navale, Y. H.; Tayade, S. B.; Digraskar, R. V.; Patil, V. B.; Kumbhar, A. S.; Sathe, B. R. Heterostructural CuO−ZnO Nanocomposites: A Highly Selective Chemical and Electrochemical NO_2 Sensor. *ACS Omega* **2019**, *4*, 20129−20141.

(13) Xing, H.; Lie, L.; Guo, Z.; Zhao, D.; Li, X.; Liu, Z. Exposing the Photocorrosion Mechanism and Control Strategies of a CuO Photocathode. *Inorg. Chem. Front.* **2019**, *6*, 2488−2499.

(14) Panzeri, G.; Cristina, M.; Jagadeesh, M. S.; Bussetti, G.; Magagnin, L. Modification of Large Area Cu_2O/CuO Photocathode with CuS Non-Noble Catalyst for Improved Photocurrent and Stability. *Sci. Rep.* **2020**, *10*, 18730.

(15) Masudy-Panah, S.; Siavash Moakhar, R.; Chua, C. S.; Kushwaha, A.; Dalapati, G. K. Stable and Efficient CuO Based Photocathode through Oxygen-Rich Composition and Au−Pd Nanostructure Incorporation for Solar-Hydrogen Production. *ACS Appl. Mater. Interfaces* **2017**, *9*, 27596−27606.

(16) Aktar, A.; Ahmmed, S.; Hossain, J.; Ismail, A. B. M. Solution-Processed Synthesis of Copper Oxide (Cu_xO) Thin Films for Efficient Photocatalytic Solar Water Splitting. *ACS Omega* **2020**, *5*, 25125−25134.

(17) Deng, M.-J.; Wang, C.-C.; Ho, P.-J.; Lin, C.-M.; Chen, J.-M.; Lu, K.-T. Facile Electrochemical Synthesis of 3D Nano-Architectured CuO Electrodes for High-Performance Supercapacitors. *J. Mater. Chem. A* **2014**, *2*, 12857−12865.

(18) Liu, Y.; Ying, Y.; Mao, Y.; Gu, L.; Wang, Y.; Peng, X. CuO Nanosheets/RGO Hybrid Lamellar Films with Enhanced Capacitance. *Nanoscale* **2013**, *5*, 9134.

(19) Fang, Z.; Rehman, S. u.; Sun, M.; Yuan, Y.; Jin, S.; Bi, H. Hybrid NiO−CuO Mesoporous Nanowire Array with Abundant Oxygen Vacancies and a Hollow Structure as a High-Performance Asymmetric Supercapacitor. *J. Mater. Chem. A* **2018**, *6*, 21131−21142.

(20) Luan, V. H.; Han, J. H.; Kang, H. W.; Lee, W. Highly Porous and Capacitive Copper Oxide Nanowire/Graphene Hybrid Carbon Nanostructure for High-Performance Supercapacitor Electrodes. *Compos. Part B Eng.* **2019**, *178*, 107464.

(21) Barai, H. R.; Lopa, N. S.; Ahmed, F.; Khan, N. A.; Ansari, S. A.; Joo, S. W.; Rahman, M. M. Synthesis of Cu-Doped Mn_3O_4@Mn-Doped CuO Nanostructured Electrode Materials by a Solution Process for High-Performance Electrochemical Pseudocapacitors. *ACS Omega* **2020**, *5*, 22356−22366.

(22) Kidowaki, H.; Oku, T.; Akiyama, T. Fabrication and Characterization of CuO/ZnO Solar Cells. *J. Phys. Conf. Ser.* **2012**, *352*, No. 012022.

(23) Fujimoto, K.; Oku, T.; Akiyama, T.; Suzuki, A. Fabrication and Characterization of Copper Oxide-Zinc Oxide Solar Cells Prepared by Electrodeposition. *J. Phys. Conf. Ser.* **2013**, *433*, No. 012024.

(24) Bhunia, R.; Dolai, S.; Dey, R.; Das, S.; Hussain, S.; Bhar, R.; Pal, A. K. Fabrication and Characterization of Cu/Cu_2O/CuO/ZnO/Al−ZnO/Ag Heterojunction Solar Cells. *Semicond. Sci. Technol.* **2018**, *33*, 105007.

(25) Iqbal, K.; Ikram, M.; Afzal, M.; Ali, S. Efficient, Low-Dimensional Nanocomposite Bilayer CuO/ZnO Solar Cell at Various Annealing Temperatures. *Mater. Renew. Sustain. Energy* **2018**, *7*, 4.

(26) Lam, N. D. Modelling and Numerical Analysis of ZnO/CuO/Cu_2O Heterojunction Solar Cell Using SCAPS. *Eng. Res. Express* **2020**, *2*, No. 025033.

(27) Kim, S.; Kim, C.-H.; Lee, S. K.; Jeong, J.-H.; Lee, J.; Jin, S.-H.; Shin, W. S.; Song, C. E.; Choi, J.-H.; Jeong, J.-R. Highly Efficient Uniform ZnO Nanostructures for an Electron Transport Layer of Inverted Organic Solar Cells. *Chem. Commun.* **2013**, *49*, 6033.
(28) Ma, J.; Lin, Z.; Guo, X.; Zhou, L.; Su, J.; Zhang, C.; Yang, Z.; Chang, J.; Frank Liu, S.; Hao, Y. Low-Temperature Solution-Processed ZnO Electron Transport Layer for Highly Efficient and Stable Planar Perovskite Solar Cells with Efficiency Over 20%. *Sol. RRL* **2019**, *3*, 1900096.
(29) Chi, D.; Huang, S.; Yue, S.; Liu, K.; Lu, S.; Wang, Z.; Qu, S.; Wang, Z. Ultra-Thin ZnO Film as an Electron Transport Layer for Realizing the High Efficiency of Organic Solar Cells. *RSC Adv.* **2017**, *7*, 14694−14700.
(30) Dehghan, M.; Behjat, A. Deposition of Zinc Oxide as an Electron Transport Layer in Planar Perovskite Solar Cells by Spray and SILAR Methods Comparable with Spin Coating. *RSC Adv.* **2019**, *9*, 20917−20924.
(31) Malwal, D.; Gopinath, P. CuO-ZnO Nanosheets with p-n Heterojunction for Enhanced Visible Light Mediated Photocatalytic Activity. *ChemistrySelect* **2017**, *2*, 4866−4873.
(32) Ahmmed, S.; Aktar, A.; Tabassum, S.; Rahman, M. H.; Rahman, M. F.; Md. Ismail, A. B. CuO Based Solar Cell with V_2O_5 BSF Layer: Theoretical Validation of Experimental Data. *Superlattices Microstruct.* **2021**, *151*, 106830.
(33) Wang, P.; Zhao, X.; Li, B. ZnO-Coated CuO Nanowire Arrays: Fabrications, Optoelectronic Properties, and Photovoltaic Applications. *Opt. Express* **2011**, *19*, 11271.
(34) Naveena, D.; Logu, T.; Sethuraman, K.; Bose, A. C. Significant Enhancement of Photo-Physicochemical Properties of Yb Doped Copper Oxide Thin Films for Efficient Solid-State Solar Cell. *J. Alloys Compd.* **2019**, *795*, 187−196.
(35) Bhaumik, A.; Haque, A.; Karnati, P.; Taufique, M. F. N.; Patel, R.; Ghosh, K. Copper Oxide Based Nanostructures for Improved Solar Cell Efficiency. *Thin Solid Films* **2014**, *572*, 126−133.
(36) Kuddus, A.; Islam, R.; Tabassum, S.; Ismail, A. B. M. I. Synthesis of Si NPs from River Sand Using the Mechanochemical Process and Its Applications in Metal Oxide Heterojunction Solar Cells. *Silicon* **2020**, *12*, 1723−1733.
(37) Prasanna, R.; Gold-Parker, A.; Leijtens, T.; Conings, B.; Babayigit, A.; Boyen, H.-G.; Toney, M. F.; McGehee, M. D. Band Gap Tuning via Lattice Contraction and Octahedral Tilting in Perovskite Materials for Photovoltaics. *J. Am. Chem. Soc.* **2017**, *139*, 11117−11124.
(38) Ganesan, R.; Vinodhini, S. P.; Balasubramani, V.; Parthipan, G.; Sridhar, T. M.; Arulmozhi, R.; Muralidharan, R. Tuning the Band Gap of Hybrid Lead Free Defect Perovskite Nano Crystals for Solar Cell Applications. *New J. Chem.* **2019**, *43*, 15258−15266.
(39) Zhang, B.; Zheng, J.; Li, X.; Fang, Y.; Wang, L.-W.; Lin, Y.; Pan, F. Tuning Band Alignment by CdS Layers Using a SILAR Method to Enhance TiO_2/CdS/CdSe Quantum-Dot Solar-Cell Performance. *Chem. Commun.* **2016**, *52*, 5706−5709.
(40) Tailor, N. K.; Abdi-Jalebi, M.; Gupta, V.; Hu, H.; Dar, M. I.; Li, G.; Satapathi, S. Recent Progress in Morphology Optimization in Perovskite Solar Cell. *J. Mater. Chem. A* **2020**, *8*, 21356−21386.
(41) Ahmmed, S.; Aktar, A.; Hossain, J.; Ismail, A. B. M. Enhancing the Open Circuit Voltage of the SnS Based Heterojunction Solar Cell Using NiO HTL. *Sol. Energy* **2020**, *207*, 693−702.
(42) Ahmmed, S.; Aktar, A.; Rahman, M. F.; Hossain, J.; Ismail, A. B. M. A Numerical Simulation of High Efficiency CdS/CdTe Based Solar Cell Using NiO HTL and ZnO TCO. *Optik (Stuttg).* **2020**, *223*, 165625.
(43) Ahmmed, S.; Aktar, A.; Rahman, M. H.; Hossain, J.; Ismail, A. B. M. Design and Simulation of a High-Performance $CH_3NH_3Pb(I_{1-x}Cl_x)_3$-Based Perovskite Solar Cell Using a CeO_x Electron Transport Layer and NiO Hole Transport Layer. *Semicond. Sci. Technol.* **2021**, *36*, No. 035002.
(44) Cheng, F.; Wu, Y.; Shen, Y.; Cai, X.; Li, L. Enhancing the Performance and Stability of Organic Solar Cells Using Solution Processed MoO_3 as Hole Transport Layer. *RSC Adv.* **2017**, *7*, 37952−37958.
(45) Song, J.; Hu, W.; Li, Z.; Wang, X.-F.; Tian, W. A Double Hole-Transport Layer Strategy toward Efficient Mixed Tin-Lead Iodide Perovskite Solar Cell. *Sol. Energy Mater. Sol. Cells* **2020**, *207*, 110351.
(46) Mamun, A. A.; Ava, T. T.; Abdel-Fattah, T. M.; Jeong, H. J.; Jeong, M. S.; Han, S.; Yoon, H.; Namkoong, G. Effect of Hot-Casted NiO Hole Transport Layer on the Performance of Perovskite Solar Cells. *Sol. Energy* **2019**, *188*, 609−618.
(47) Yin, X.; Guo, Y.; Xie, H.; Que, W.; Kong, L. B. Nickel Oxide as Efficient Hole Transport Materials for Perovskite Solar Cells. *Sol. RRL* **2019**, *3*, 1900001.
(48) Kasinathan, D.; Ashok, M. *Microwave Assisted WO3 Hole Transport Material for Stable Perovskite Solar Cell*. In *AIP Conference Proceedings*; 2020; Vol. *2265*, p 030648.
(49) Li, Z. Stable Perovskite Solar Cells Based on WO_3 Nanocrystals as Hole Transport Layer. *Chem. Lett.* **2015**, *44*, 1140−1141.
(50) Guo, Y.; Lei, H.; Xiong, L.; Li, B.; Chen, Z.; Wen, J.; Yang, G.; Li, G.; Fang, G. Single Phase, High Hole Mobility Cu_2O Films as an Efficient and Robust Hole Transporting Layer for Organic Solar Cells. *J. Mater. Chem. A* **2017**, *5*, 11055−11062.
(51) Chatterjee, S.; Pal, A. J. Introducing Cu_2O Thin Films as a Hole-Transport Layer in Efficient Planar Perovskite Solar Cell Structures. *J. Phys. Chem. C* **2016**, *120*, 1428−1437.
(52) Elumalai, N. K.; Saha, A.; Vijila, C.; Jose, R.; Jie, Z.; Ramakrishna, S. Enhancing the Stability of Polymer Solar Cells by Improving the Conductivity of the Nanostructured MoO_3 Hole-Transport Layer. *Phys. Chem. Chem. Phys.* **2013**, *15*, 6831.
(53) Hu, X.; Chen, L.; Chen, Y. Universal and Versatile MoO_3-Based Hole Transport Layers for Efficient and Stable Polymer Solar Cells. *J. Phys. Chem. C* **2014**, *118*, 9930−9938.
(54) Kuddus, A.; Rahman, M. F.; Ahmmed, S.; Hossain, J.; Ismail, A. B. M. Role of Facile Synthesized V_2O_5 as Hole Transport Layer for CdS/CdTe Heterojunction Solar Cell: Validation of Simulation Using Experimental Data. *Superlattices Microstruct.* **2019**, *132*, 106168.
(55) Zhang, L.; Jiang, C.; Wu, C.; Ju, H.; Jiang, G.; Liu, W.; Zhu, C.; Chen, T. V_2O_5 as Hole Transporting Material for Efficient All Inorganic Sb_2S_3 Solar Cells. *ACS Appl. Mater. Interfaces* **2018**, *10*, 27098−27105.
(56) Terán-Escobar, G.; Pampel, J.; Caicedo, J. M.; Lira-Cantú, M. Low-Temperature, Solution-Processed, Layered V_2O_5 Hydrate as the Hole-Transport Layer for Stable Organic Solar Cells. *Energy Environ. Sci.* **2013**, *6*, 3088.
(57) Greiner, M. T.; Helander, M. G.; Tang, W.-M.; Wang, Z.-B.; Qiu, J.; Lu, Z.-H. Universal Energy-Level Alignment of Molecules on Metal Oxides. *Nat. Mater.* **2012**, *11*, 76−81.
(58) Potscavage Jr, W. J.; Sharma, A.; Kippelen, B. Critical Interfaces in Organic Solar Cells and Their Influence on the Open-Circuit Voltage. *Acc. Chem. Res.* **2009**, *42*, 1758−1767.
(59) Steim, R.; Kogler, F. R.; Brabec, C. J. Interface Materials for Organic Solar Cells. *J. Mater. Chem.* **2010**, *20*, 2499.
(60) Roy, S. C.; Varghese, O. K.; Paulose, M.; Grimes, C. A. Toward Solar Fuels: Photocatalytic Conversion of Carbon Dioxide to Hydrocarbons. *ACS Nano* **2010**, *4*, 1259−1278.
(61) Chen, Y.; Wang, Y.; Wang, R.; Hu, X.; Tao, J.; Weng, G.-E.; Zhao, C.; Chen, S.; Zhu, Z.; Chu, J.; Akiyama, H. Importance of Interfacial Passivation in the High Efficiency of Sb_2Se_3 Thin-Film Solar Cells: Numerical Evidence. *ACS Appl. Energy Mater.* **2020**, *3*, 10415−10422.
(62) Stolterfoht, M.; Caprioglio, P.; Wolff, C. M.; Márquez, J. A.; Nordmann, J.; Zhang, S.; Rothhardt, D.; Hörmann, U.; Amir, Y.; Redinger, A.; Kegelmann, L.; Zu, F.; Albrecht, S.; Koch, N.; Kirchartz, T.; Saliba, M.; Unold, T.; Neher, D. The Impact of Energy Alignment and Interfacial Recombination on the Internal and External Open-Circuit Voltage of Perovskite Solar Cells. *Energy Environ. Sci.* **2019**, *12*, 2778−2788.
(63) Hernńdez-Como, N.; Morales-Acevedo, A. Simulation of Hetero-Junction Silicon Solar Cells with AMPS-1D. *sol. Energy Mater. Sol. Cells* **2010**, *94*, 62−67.

https://doi.org/10.1021/acsomega.1c00678
ACS Omega 2021, 6, 12631−12639

(64) Hossain, E. S.; Chelvanathan, P.; Shahahmadi, S. A.; Sopian, K.; Bais, B.; Amin, N. Performance Assessment of Cu_2SnS_3(CTS) Based Thin Film Solar Cells by AMPS-1D. *Curr. Appl. Phys.* **2018**, *18*, 79−89.
(65) Belarbi, M.; Beghdad, M.; Mekemeche, A. Simulation and Optimization of N-Type Interdigitated Back Contact Silicon Heterojunction (IBC - SiHJ) Solar Cell Structure Using Silvaco Tcad Atlas. *Sol. Energy* **2016**, *127*, 206−215.
(66) Ali, K.; Khan, S. A.; MatJafri, M. Z. TCAD Design of Silicon Solar Cells in Comparison of Antireflection Coatings and Back Surface Field. *Optik (Stuttg).* **2016**, *127*, 7492−7497.
(67) Cho, S.-P.; Yeo, J.-S.; Kim, D.-Y.; Na, S.; Kim, S.-S. Brush Painted V_2O_5 Hole Transport Layer for Efficient and Air-Stable Polymer Solar Cells. *Sol. Energy Mater. Sol. Cells* **2015**, *132*, 196−203.
(68) Zilberberg, K.; Trost, S.; Schmidt, H.; Riedl, T. Solution Processed Vanadium Pentoxide as Charge Extraction Layer for Organic Solar Cells. *Adv. Energy Mater.* **2011**, *1*, 377−381.
(69) Straub, A.; Gebs, R.; Habenicht, H.; Trunk, S.; Bardos, R. A.; Sproul, A. B.; Aberle, A. G. Impedance Analysis: A Powerful Method for the Determination of the Doping Concentration and Built-in Potential of Nonideal Semiconductor *p-n* Diodes. *J. Appl. Phys.* **2005**, *97*, No. 083703.
(70) Kim, G. W.; Shinde, D. V.; Park, T. Thickness of the Hole Transport Layer in Perovskite Solar Cells: Performance versus Reproducibility. *RSC Adv.* **2015**, *5*, 99356−99360.
(71) Zhan, Z.; Cao, J.; Xie, W.; Hou, L.; Ye, Q.; Liu, P. Role of Vanadium Pentoxide Hole-Extracting Nanolayer in Rubrene/C_{70}-Based Small Molecule Organic Solar Cells. *J. Nanomater.* **2014**, *2014*, 1−7.
(72) Chen, J.; Park, N.-G. Causes and Solutions of Recombination in Perovskite Solar Cells. *Adv. Mater.* **2019**, *31*, 1803019.
(73) Wang, F.; Bai, S.; Tress, W.; Hagfeldt, A.; Gao, F. Defects Engineering for High-Performance Perovskite Solar Cells. *npj Flex. Electron.* **2018**, *2*, 22.
(74) Huang, J.; Yuan, Y.; Shao, Y.; Yan, Y. Understanding the Physical Properties of Hybrid Perovskites for Photovoltaic Applications. *Nat. Rev. Mater.* **2017**, *2*, 17042.

https://doi.org/10.1021/acsomega.1c00678
ACS Omega 2021, 6, 12631−12639